Optimization of Structural Parameters of PCF Polarization Filter by a Genetic Algorithm

Dan Yang, *Member, IEEE*, Zhulin Wei, Huobin Qin, Bin Xu, and Tonglei Cheng

***Abstract*—The material and geometry of photonic crystal fiber (PCF) are significant adjustable characteristics, and affect its optical properties. Finding the global optimal fiber is formulated as an optimization problem, and intelligent algorithms are used for the complex objective optimization. This paper presents the optimal structure of PCF for polarization filter determined by the Genetic Algorithm (GA) method, and the fitness function of GA is defined relatedly to the polarization filter optical index crosstalk (CT) and bandwidth. The designed PCF polarization filter has the following characteristics: the CT reaches 1845.3113 dB at 1.55 μm. When the fiber length is limited to 1000 nm, the bandwidth value exceeds 800 nm. Numerical results demonstrate that the performance of the designed PCF filter is better than that of the original and also have proved the GA method is beneficial to the design and fabrication of optical fibers.**

***Index Terms*—Photonic crystal fiber, intelligent algorithms, polarization filter, genetic algorithm.**

I. Introduction

PHOTONIC crystal fiber (PCF), first reported in 1996, has aroused generated great interest among researchers thanks to the new ways of controlling and guiding light [1]. Distinct from conventional optical fibers, PCF is usually formed from silica with regularly arranged microscopic air holes running along its length, playing the role of cladding, and the core is considered as a defect region [2]. The remarkable wavelength-dependent property of the refractive index of the cladding, combined with the high refractive index contrast between silica and air, provides a set of new interesting features. Because of its unique properties of large mode area, non-linearity, high birefringence and structural flexibility, PCF has broad application prospects in biosensor, polarization filter, fiber laser, directional couplers, etc.

Manuscript received 28 September 2022; accepted 7 November 2022. Date of publication 10 November 2022; date of current version 22 November 2022. This work was supported in part by the National Natural Science Foundation of China under Grants U22A20221, 61836011, and 71790614, in part by the Fundamental Research Funds for the Central Universities under Grant 2020GFZD008, in part by the 111 Project under Grant B16009, in part by the Natural Science Foundation of Liaoning Province under Grant 2021-MS093, and in part by the Basic Scientific Research Project of the Education Department of Liaoning Province in 2021under Grant LJKZ0014. *(Corresponding author: Tonglei Cheng.)*

Dan Yang, Zhulin Wei, Huobin Qin, and Tonglei Cheng are with the College of Information Science and Engineering, Northeastern University, Shenyang, Liaoning 110819, China (e-mail: yangdan@mail.neu.edu.cn; 2070810@stu.neu.edu.cn; 20205299@stu.neu.edu.cn; chengtonglei@ise.neu.edu.cn).

Bin Xu is with the School of Computer Science and Engineering, Northeastern University, Shenyang, Liaoning 110819, China (e-mail: xubin@mail.neu.edu.cn).

Digital Object Identifier 10.1109/JPHOT.2022.3221095

The physical structure and material properties of PCF are a significant design part, which is responsible for optical properties. Many research works have been reported to solve this problem, especially for the PCF polarization filter. In 2020, Aslam Mollah et al. [3] presented a single-polarization filter based on high birefringence (Hi-Bi) PCFs composed of copper microwires. Copper is chemically stable and is more advantageous to manufacture using fine wire than any metal-coated PCF. Furthermore, the proposed filter can be efficiently implemented at any wavelength of the optical communication window by optimizing the structural parameters. In 2021, Qiao et al. [4] proposed a tunable dual-band metamaterial filter composed of two identical metal split rings with different angles. The operating frequency variation range can reach 2.5 GHz with the rotation angle varying from 30°–90°. All the results validate the tunable properties of the proposed metamaterial filter. In 2022, Yu et al. [5] demonstrated a high CT and large bandwidth PCFs polarization filter. An asymmetric leakage channel structure is introduced in the y polarization direction, intensifying the energy leakage to the outer cladding, resulting in a higher polarization extinction ratio. The proposed PCF has broad application prospects in the fields of optical information processing and optical fiber communication. All the above studies perform the optimal fiber structure for new properties of PCF polarization by adjusting parameters. The complexity of designed PCF has a significant effect on parameter solution speed. More exhaustive steps are required to obtain optimal parameters when dealing with hybrid structures [6]. The design process is computationally intensive, and time-consuming [7].

The simulated and designed way of photonic systems are will usher in a data science revolution, which covers a wide range of topics including neuromorphic computing, inverse design of photonic devices and many other emerging applications [8], [9]. Intelligent algorithms provide a powerful alternative approach for complex parameter optimization. The genetic algorithm (GA) [10] is a well-known intelligent optimal algorithm widely used in factory production schedule and vehicle route planning for optimal arrangement. There exist considerable parameter options problems for optical fiber device applications, and some researchers have used GA to design optical fibers or devices. Tao et al. [11] proposed a fault diagnosis method based on a deep belief network optimized by GA to prevent the problem from falling into local optimum. The results show that the proposed method significantly improves the identification accuracy of photovoltaic array faults. Lu et al. [12] applied GA on PCFs, which enables it to provide intense light confinement and a small

half-diffraction angle of the output beam. Finally, it is confirmed that the half-diffraction angle of the output beam of PCFs can be reduced. Arteaga-Sierra et al. [13] employed GA to design a fiber based on a dual pulse light source that displays two predefined spectral peaks in the state of anomalous group velocity dispersion. It enables control of SC dynamics in a wide range of situations. Huang et al. [14] combine GA with Mie theory to optimize the magnetic field intensity distribution of photonic nanojets (PNJs) generated at visible wavelengths in free space. The adequately designed five-layer micropillar structures can generate ultralong PNJs. Furthermore, a PNJ with a full width of $\sim 0.22\,\lambda_0$ can be obtained outside the optimized microcylindrical surface. Although these works have made significant progress in the performance of PCF devices, more efforts about PCF structures are still needed to be conducted before PCF practical fabrication applications.

In this work, we present an application of the GA as a novel method of PCF structure design for polarization filter in the field of optical communication. The GA is used to optimize the air hole arrangement and size for PCF. The chromosomes represent the PCF structure parameters, and the fitness function is defined to be related to the optical indexes, the crosstalk and bandwidth. Then, through selection, crossover and mutation, the possible optimal PCF structure will be found in large-scale search space based on the maximum of a given fitness function. Using numerical simulations, the performance of the designed PCF is evaluated by univariate and bivariate fitness functions separately. When CT is used as the variable of the fitness function, CT reaches 1775.5735 dB and the bandwidth is 850nm. Then, when CT and bandwidth are used both as the variables of the fitness function, CT reaches 1845.3113 dB, and the bandwidth is more significant than 800 nm. Furthermore, considerations about PCF filter by GA optimization in fabrication are also discussed. Thus, by adjusting the structure by GA, a better PCF polarization filter can be designed.

II. Methods

A. PCF Principles

The propagation of light in a medium must satisfy Maxwell's equations, and the study of PCF is no exception [15]. According to Maxwell's equations, the vector wave equation corresponding to the electromagnetic field in the PCF is derived as:

$$\nabla \times \left(\frac{1}{\mu_r}\nabla \times \vec{E}\right) - k_0^2\,\varepsilon_r\,\vec{E} = 0 \tag{1}$$

Where $\vec{E}$ is the electric field, ε_r and μ_r are the relative permittivity and relative permeability, respectively.

Based on the standard variational principle, the corresponding function of (1) is:

$$F\left(\vec{E}\right) = \frac{1}{2}\iint_{\Omega}\left[\frac{1}{\mu_r}\left(\nabla\times\vec{E}\right)\left(\nabla\times\vec{E}\right)^{*} - k_0^2\,\varepsilon_r\vec{E}\vec{E}^{*}\right]d\Omega \tag{2}$$

Where Ω represents the area of fiber cross-section. In case the electric field is expressed as:

$$\vec{E}\,(x,y,z) = \vec{E}\,(x,y)\,e^{-jk_z z} \tag{3}$$

Where k_z is the propagation constant. By substituting (3) into (2), it can be obtained:

$$F\left(\vec{E}\right) = \frac{1}{2}\iint_{\Omega}\left[\frac{1}{\mu_r}\left(\nabla_t\times\vec{E}_t\right)\left(\nabla_t\times\vec{E}_t\right)^{*} - k_0^2\,\varepsilon_r\vec{E}\vec{E}^{*} + \frac{1}{\mu_r}\left(\nabla_t\times\vec{E}_z + jk_z\vec{E}_t\right)\left(\nabla_t\times\vec{E}_z + jk_z\vec{E}_t\right)^{*}\right]d\Omega \tag{4}$$

Where ∇_t stands for transverse operator, $\vec{E}_t$ and $\vec{E}_z$ represent the transverse and axial components of the electric field, respectively.

By multiplying (4) by k_z^2 and substituting variables $\overrightarrow{e_t} = k_z\vec{E}_t, e_z = -jE_z$. By using global coding and the Ritz variation method with complex-valued problems, the generalized eigenvalue equation is obtained. By solving the eigenvalue equation, the corresponding eigenvalues and eigenvectors can be obtained, where the eigenvalues correspond to the propagation constant of light. The optical parameters were achieved by mode analysis based on eigen solutions.

The performance of the PCF polarization filter is based on the modal losses of the two polarized modes, which can be calculated as follows [16]:

$$Loss\,(dB/cm) = 8.686\times 2\pi\times Im\,(neff)\times 10^4/\lambda \tag{5}$$

Where $Im(neff)$ denotes the imaginary part of effective refractive index and λ denotes the operating wavelength.

The CT and bandwidth are standard evaluation metrics in the field of polarization filter. According to the principle of polarization filtering, CT is a specific parameter used to evaluate the transmission performance of polarization filter while characterizing the influence of unnecessary polarization modes [17]. CT can be defined by using the following equation:

$$\mathrm{CT} = 20\lg\left\{\exp\left(\alpha_2 - \alpha_1\right)L\right\} \tag{6}$$

Where α_2 and α_1 represent the confinement losses of y polarization and x polarization modes, respectively, and L represents the length of the fiber. The available optical bandwidth is expressed by the corresponding wavelength range when CT exceeds 20 dB or falls below -20 dB [18]. The design of the PCF polarization filter is to obtain the optimal optical parameters by discussing the structure, which is regarded as a problem of parameter optimization.

B. GA Basics

GA is usually used in computing to find exact or approximate solutions to optimization and search problems [19]. It is an adaptive probabilistic optimization technology suitable for the optimization of complex systems based on biological genetics and evolutionary mechanisms. According to the law of survival of the fittest in nature, the genes of outstanding individuals in

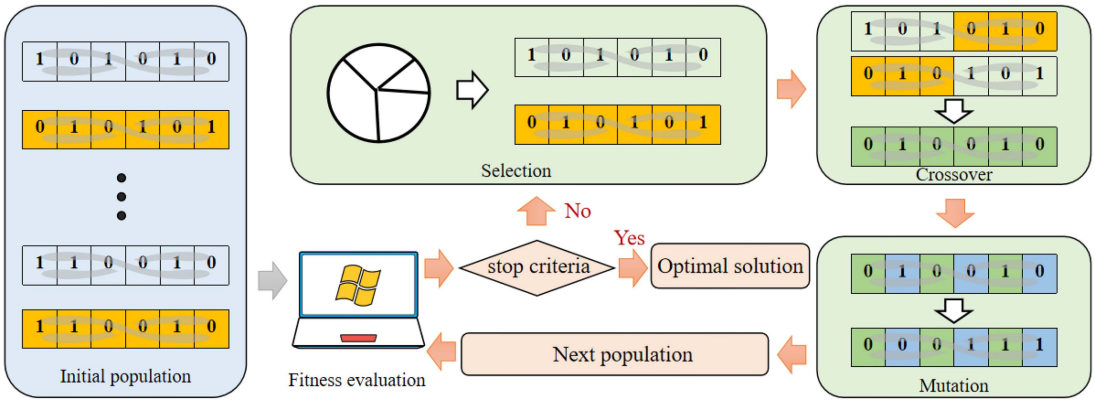

Fig. 1. The schematic of GA.

the population are inherited [20]. The chromosomes of each individual generate new chromosomes with more excellent fitness through selection, crossover and mutation. The optimal solution to the target problem can be obtained by continuously optimizing the population through repeated iterations. Compared with other optimization algorithms, GA has the advantages of not quickly falling into local optimum, fast calculation speed and easy operation, and can calculate more complex problems simultaneously.

The schematic of GA is shown in Fig. 1. An initial population from the space of the possible solutions is generated for the research problem first. Each individual is encoded in some form as a string, usually called chromosome [21]. Next, the fitness of chromosome individuals is evaluated through the numerical model of practical problem. The chromosome individuals in the population are further selected and inherited based on their fitness through three operations of selection, crossover and mutation. The selection is to choose the better individuals from the current population based on the fitness value of chromosome individuals, and give the opportunity to breed the new individual for the next generation. The crossover is the exchange of gene segments at two intersections to create a new individual from a random pair of individuals from the previous generation [22]. The operation retains excellent genes. The mutation means that each locus of a chromosome has a certain probability of change, which is by exchanging the gene segments of the chromosome with some allele segments. After the above three operations, a new population will be generated, and the fitness function will be evaluated repeatedly, and then the population will update again by the three operations. The iterative process is repeated until the population criteria meet a specific index or the set number of iterations is completed [23]. As a consequence, GA will obtain a global optimal solution in research space.

C. Optimization of the PCF Structure Parameters Using Genetic Algorithm

In this paper, GA is proposed to determine the structure of PCF polarization filter starting from the optical properties desired for polarization filter application. The main operations of the genetic algorithm are as follows:

A chromosome or an array of variable values will be defined by GA. If the chromosome has N_{var} parameters of PCF given by $\mathrm{q}_1,\ \mathrm{q}_2, \mathrm{q}_3 \ldots \mathrm{q}_{N_{val}}$, then the chromosome is written as an N_{var} element row vector.

$$chromosome\ =\ [\mathrm{q}_1,\ \mathrm{q}_2, \mathrm{q}_3 \ldots \mathrm{q}_{N_{val}}] \tag{7}$$

Here, chromosomes represent the structural and material parameters of PCF: $[s,\ \mathrm{t}, p, \mathrm{d}_1, \mathrm{d}_2, \mathrm{d}_3, \mathrm{d}_4]$ and the value of the gene is limited to the given range of each parameter.

Each chromosome has a fitness value evaluated by the fitness function:

$$fitness\ =\ f\,(CT,\ BW) \tag{8}$$

The selection of the fitness function is related to the optical characteristics of CT and BW. In the calculation process, the values of the two are the historical values during the operation of the algorithm.

GA starts with a set of chromosomes called population. The population has N_{pop} chromosomes is initially set to: $s\ =\ 3.2\ \mu\mathrm{m},\ t\ =\ 21.0\ \mathrm{nm},\ p\ =\ 1.85\ \mu\mathrm{m},\ \mathrm{d}_1 = 1.6\ \mu\mathrm{m},\ \mathrm{d}_2 = 1.5\ \mu\mathrm{m},\ \mathrm{d}_3 = 1.4\ \mu\mathrm{m},\ \mathrm{d}_4 = 1.0\ \mu\mathrm{m}$. At this time, the PCF filter has a small CT peak of 407.8167 dB at 1.55 μm, which is convenient for algorithm optimization.

For every generation, GA performs the following operations according to the current population:

Step 1: Compute the fitness of each individual in the population.

The value of each gene on a single chromosome is set as the parameter of COMSOL model, and the desired optical properties are obtained through the model solution. The corresponding fitness function is designed according to the desired optical properties. The value of the optical property is proportional to the fitness value. Suppose $f_i(i\ =\ 1,\ 2,\ 3, \ldots N_{pop})$ is the fitness of the i_{th} individual.

Step 2: Select operation.

Selection is chosen based on fitness. The fitness is sorted from high to low, and the first $N_{parents}$ chromosomes are selected as parents. This is because chromosomes with higher fitness contain better traits to ensure that offspring are more likely to

inherit and produce superior traits, while other chromosomes with low fitness are deleted. In this way, the chromosomes with higher fitness are always left in each generation of the population, which drives the entire population to evolve towards a direction with better fitness.

Step 3: Crossover operation.

The offspring are generated using a single-point crossover technique. Firstly, the crossover probability p_{cross} is specified. And then, a random number $prob \in [0,\ 1]$ is generated by randomly selecting two chromosomes in the parent. If $prob < p_{cross}$, crossover occurs:

The chromosome is divided into two parts by picking a point at random, and then the two chromosomes exchange some genes to produce a new offspring chromosome (the parents retained). An example of the process is as follows:

$$\begin{matrix} \text{Crossoverpoint} \\ \downarrow \\ parent1 : [3.2,\ 21.0,\ 1.85,\ 1.6,\ 1.5,\ 1.4,\ 1.0] \end{matrix} \tag{9}$$

$$parent2 :\ [3.1,\ 21.0,\ 1.94,\ 1.8,\ 1.7,\ 1.6,\ 1.1] \tag{10}$$

The chromosomes generated after crossover operation:

$$offspring1 :\ [3.2,\ 21.0,\ 1.85,\ 1.6,\ 1.7,\ 1.6,\ 1.1] \tag{11}$$

$$offspring2 :\ [3.1,\ 21.0,\ 1.94,\ 1.8,\ 1.5,\ 1.4,\ 1.0] \tag{12}$$

If $prob \geq\ p_{cross}$, crossover will not occur. And the two parents will be directly copied as progeny chromosomes. The process is repeated until the number of chromosomes in the population is restored from $N_{parents}$ to N_{pop}.

Step 4: Mutation operation.

The last step in genetic operation is mutation. The mutation probability is specified as $p_{mutation}$. For each offspring chromosome, the following operations are performed:

Each gene generates a random number $prob \in [0,\ 1]$. If $prob <\ p_{mutation}$, the gene is replaced with a random new value within the range of parameters. Otherwise, the original value is retained.

Finally, it is fully optimized until the stop criteria (if the maximum number of iterations or sufficient fitness is achieved) by repeating steps 1-4.

III. Results and Analysis

A. PCF Polarization Filter Model

The geometry of the asymmetric gold-coated PCF polarization filter in [24] is selected as the initial structure studied in this paper. Its cross-section is shown in Fig. 2, where x and y are the transversal directions, and z represents the propagation direction. There are four layers of hexagonal air holes in this structure, and s represents the distance between the gold-coated air holes and the core of fiber. p is the air hole spacing. t is the thickness of the gold film. d_1 denotes the diameter of the gold-coated hole, and the left and right sides of the center of silica core are the air holes with diameter of d_2. The outer three layers

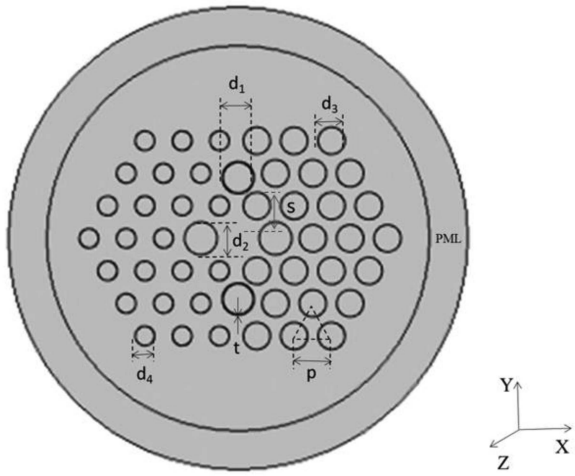

Fig. 2. Cross-section of the PCFs polarization filter.

of air holes with diameters d_3 and d_4 are introduced around the gold-coated hole, which breaks the symmetry of the structure and improves the birefringence characteristic of the filter.

Each chromosome in GA represents a set of parameters [25]. The structure of this paper contains seven geometric parameters, and the corresponding chromosome has seven genes. The parameters and the value range of the selected geometric parameters are shown in Table I. These constraints are selected based on the original structural parameters, which guarantees that all members optimized by the GA algorithm exhibit better performance than previous work.

B. Optimaization via GA

To avoid the exhaustive parameter searches and to improve the efficiency, the geometric parameters of the fiber are optimized using the appropriate optical properties as the fitness function [26].

1) Univariate Results and Analysis: The initial geometric parameters of the univariate experiments strictly met the selection range of geometric parameters given in Table I, which are shown in the first row of Table II. The fitness function is calculated from the difference of the confinement loss in the x polarization direction and the y polarization direction in the wavelength range of 1.0–2.0 μm. The value of fitness corresponding to the initial parameter group is 407.8167 dB. Combined with the communication window, they are used as a benchmark for further optimization. Under the same initial structure, the size of the population and parents are set to 32 and 16, respectively. The mutation probability is 0.2. The crossover probability is 0.4, and the number of iterations is 20.

The geometric parameter values of different generations and the corresponding fitness are shown in Table II. Due to the randomness of GA, the value of the geometric parameters is randomly selected within the given parameter range rather than adjacent when mutation occurs. At the same time, the complexity of the fitness function leads to discontinuities in the results.

TABLE I
THE VALUE RANGE AND ACCURACY OF GEOMETRIC PARAMETERS

parameters	s (μm)	t (nm)	p (μm)	d_1 (μm)	d_2 (μm)	d_3 (μm)	d_4 (μm)
range	3.0 - 3.3	19 - 25	1.85 - 2.15	1.5 - 1.8	1.3 - 1.9	1.2 - 1.8	0.9 - 1.2

TABLE II
DIFFERENT GENERATIONS OF GA SOLUTIONS BASED ON CT

generation	s (μm)	t (nm)	p (μm)	d_1 (μm)	d_2 (μm)	d_3 (μm)	d_4 (μm)	fitness(dB)
1	3.2	21	1.85	1.6	1.5	1.4	1.0	407.8167
2	3.2	22	1.85	1.6	1.7	1.4	1.0	545.8949
3	3.2	22	1.85	1.6	1.7	1.4	1.0	545.8949
4	3.1	21	1.87	1.6	1.5	1.4	1.0	991.8978
7	3.1	21	1.87	1.6	1.5	1.4	1.0	991.8978
8	3.1	21	1.87	1.6	1.5	1.4	1.0	991.8978
10	3.1	21	1.87	1.6	1.5	1.4	1.0	991.8978
14	3.1	21	1.87	1.7	1.5	1.4	1.0	1775.4735
16	3.1	21	1.87	1.7	1.5	1.4	1.0	1775.4735

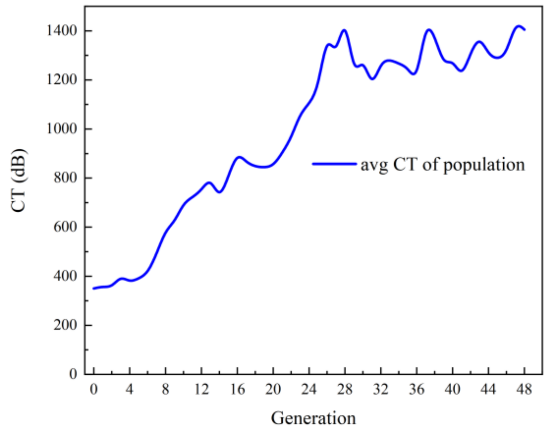

Fig. 3. The average CT value of each generation of the population.

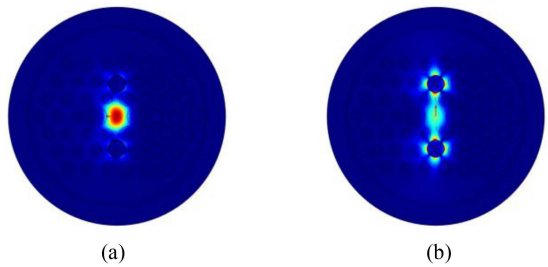

Fig. 4. The electric field distribution of the 14th generation. (a) X polarization. (b) Y polarization.

The above two factors cause algebra of the maximum fitness to appear randomly. However, the fitness of the whole population showed an upward trend in general. The average CT value of each generation of the population is shown in Fig. 3. It can be seen from Fig. 3 that the maximum fitness value was uncertain due to the influence of random factors. The most representative generations are selected for analysis: the 1st, 2nd, 4th, and 14th generations.

The electric field distribution of the 14th generation is presented in Fig. 4. The energy of electric field in the x polarization direction is completely confined at the core, and the y polarization direction leaks a small part. As the number of generations increases, the leakage in the y polarization direction increases gradually.

Fig. 5 depicts the optical curve of the 1st, 2nd, 4th and 14th generations. Fig. 5(a) is the corresponding confinement losses spectra of x and y polarization direction core modes. The solid and dashed lines represent the confinement loss in the y polarization and x polarization directions, respectively. At 1.55 μm, the peak value of y polarization direction confinement loss shows a rising trend from generation to generation, while there is little change in the x polarization direction. When the number of iterations reaches the 14th generation, the peak of y polarization confinement loss is 2052.9117 dB/cm, while the x polarization peak is 8.8223 dB/cm. The more considerable difference between the confinement loss of the x and y polarization directions indicates that the 14th generation geometric parameters can achieve filtering characteristics in a single polarization direction.

Compared with the 1st generation, the s of the 14th generation has been decreased by 0.1 μm. p, d_1 are in several increased by 0.2 μm and 0.1 μm. The increase of d_1 and the decrease of s will enhance the probability of energy conversion between the core and the gold film, thus enhancing the coupling strength and eventually leading to the increase of the confinement loss value [27]. Fig. 5(b) describes the effective refractive indices of y polarization direction core modes and SPP modes at different generations. The solid lines and the dashed lines state the real part of the effective refractive index of the core-guided mode and the SPP mode in the y polarization direction, separately. The peak position in Fig. 5(a) is the intersection of the solid lines and dashed lines in Fig. 5(b), which is the coupling point.

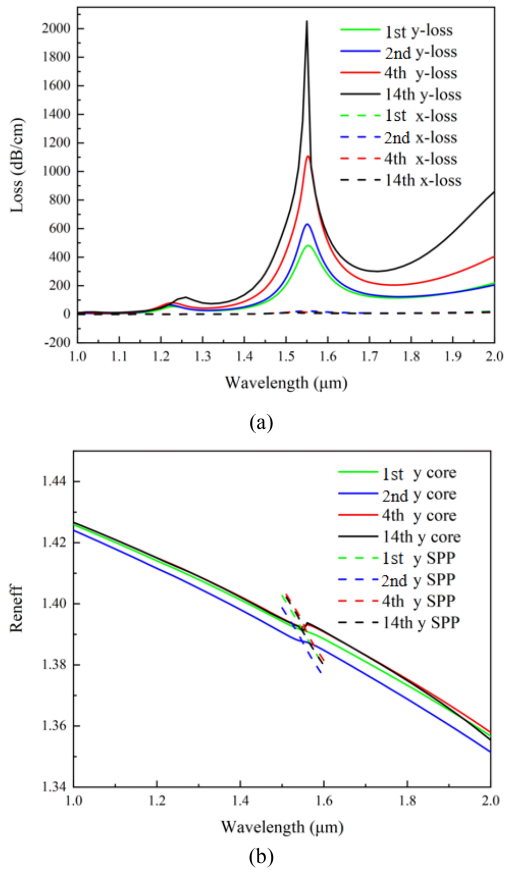

Fig. 5. The optical curve of the first, second, fourth and fourteenth generations. (a) the corresponding confinement losses spectra of x and y polarization direction core modes. (b) Effective refractive indices of y polarization direction core modes and SPP modes at different generations.

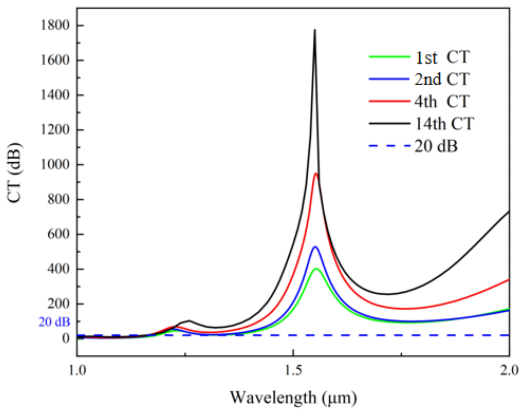

Fig. 6. The CT and bandwidth for 1000 nm fiber length of the first, second, fourth and fourteenth generations.

Fig. 6 reveals the CT (fitness function) and bandwidth for 1000 nm fiber length of the 1st, 2nd, 4th and 14th generations. The CT value at the peak is 407.8167 dB, 545.8948 dB, 991.8978 dB and 1775.4735 dB, respectively. And the bandwidth increases from 700 nm to 850 nm. The value of CT depends on the peak difference of the confinement loss between

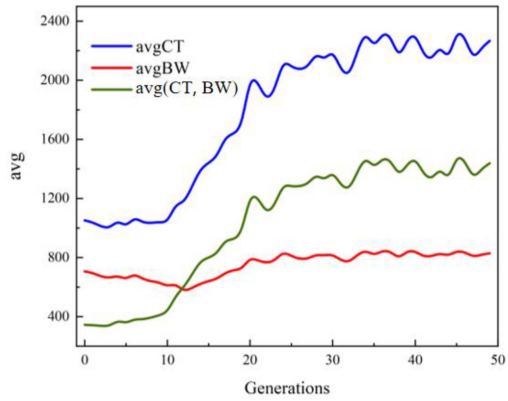

Fig. 7. The average CT, BW, (CT, BW) value of each generation of the population.

the x and y polarization directions. The bandwidth value increases with the aggrandizement of CT openings. At this point, it should be noted that in the iterative process, the selection of the optimal population is mainly based on the communication window at 1.55 μm, supplemented by the fitness function.

2) Bivariate Results and Analysis: The analysis using CT as the fitness function can only find a better CT value at 1.55 μm, and the bandwidth is obtained after obtaining the CT value data distribution. But the choice of bandwidth is not supported by data. Therefore, the combination of CT value and bandwidth is used as fitness function to discuss the influence of geometric parameters on optical properties. The selection of the communication window is also given priority. The fitness function is as follows:

$$fitness = \alpha \frac{CT - CT_{\min}}{CT_{\max} - CT_{\min}} + \beta \frac{BW - BW_{\min}}{BW_{\max} - BW_{\min}} \tag{13}$$

Where α and β are the weights. $CT_{\max}$ and $BW_{\max}$ are the maximum values of CT and bandwidth, respectively. And $CT_{\min}$ and $BW_{\min}$ are the minimum values of the two.

The settings of the GA parameters in this part are the same as the previous analysis: the number of the population and parents are 32 and 16, and the rate of mutation and crossover are 0.2 and 0.4. The difference is that the parent selection strategy is steady state selection [28]. The weights α and β are both set to 0.5 after many attempts. Table III provides the GA solutions based on different generations of CT and bandwidth. The initial population is set to $s = 3.2\,\mu$m, $t = 21$ nm, $p = 1.85\,\mu$m $d_1 = 1.6\,\mu$m, $d_2 = 1.5\,\mu$m, $d_3 = 1.4\,\mu$m, $d_4 = 1.0\,\mu$m. The fitness function value here is the difference between the normalized value of CT and bandwidth. Because the bandwidth limitation is added, the fitness value shows a certain oscillation. The value of the bandwidth depends on the change of the CT.

Fig. 7 is the curve of average value changing with the number of iterations. The blue, red and green lines represent CT, bandwidth and their sum, respectively. As seen from the figure, all three lines are basically in an upward trend. The change in CT plays a crucial role in this analysis. The values of CT and bandwidth corresponding to the maximum fitness value of each

TABLE III
DIFFERENT GENERATIONS OF GA SOLUTIONS BASED ON CROSSTALK AND BANDWIDTH

generation	s (μm)	t (nm)	p (μm)	d_1 (μm)	d_2 (μm)	d_3 (μm)	d_4 (μm)	fitness(dB)
0	3.2	21	1.85	1.6	1.5	1.4	1.0	1238.6849
1	3.2	20	1.85	1.8	1.5	1.4	1.0	2.1418181
2	3.2	21	1.97	1.8	1.5	1.4	1.0	0.9890823
3	3.2	21	1.85	1.6	1.5	1.4	1.0	0.9379815
4	3.1	21	1.98	1.8	1.5	1.4	1.0	1.2812717
5	3.2	21	2.14	1.6	1.5	1.7	1.0	1.6221886
12	3.1	21	2.01	1.8	1.9	1.4	1.0	1.8902107
13	3.1	21	1.98	1.8	1.7	1.4	1.1	2.0901241
15	3.1	21	1.94	1.8	1.7	1.5	1.0	1.9420488

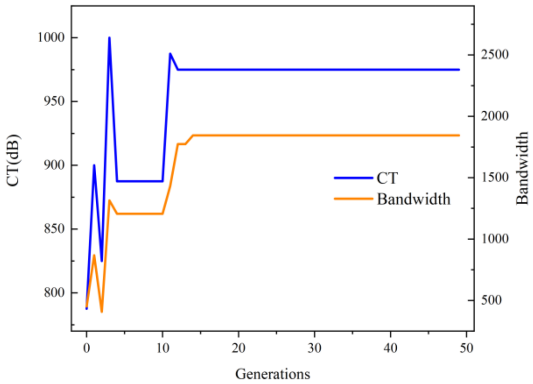

Fig. 8. The CT and bandwidth values corresponding to the maximum fitness value of 50 iterations.

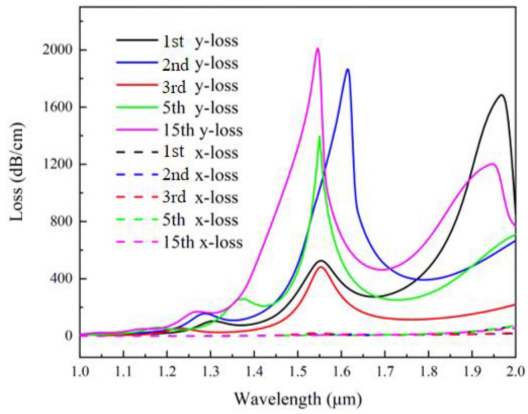

(a)

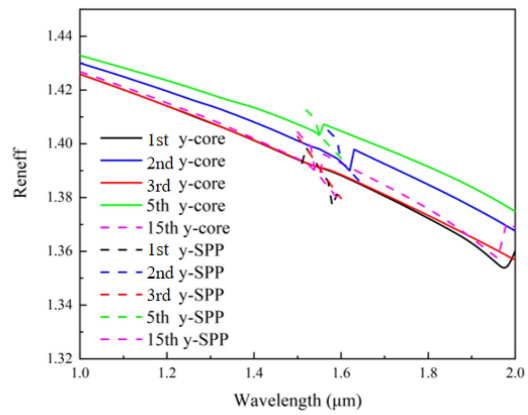

(b)

Fig. 9. The optical curve of the first, second, third, fifth and fifteenth generation. (a) the corresponding confinement losses spectra of x and y polarization direction core modes. (b) Effective refractive indices of y polarization direction core modes and SPP modes at different generations.

generation of 50 iterations are analyzed, as shown in Fig. 8. It can be seen that the value of CT and bandwidth converge within 20 generations. Therefore, the 1st, 2nd, 3rd, 5th and 15th generations are studied as changes in the optical characteristics of the analysis.

The confinement loss of the core mode and the dispersion relation of the fiber core mode, together with SPP mode are given out in the Fig. 9(a) and (b), respectively. The SPP mode can be coupled to the core-guided mode when the phase matching condition is satisfied (resonance wavelength). Furthermore, the resonance wavelength corresponds to the point where the phase is matched exactly. In Fig. 9(a), the solid and dashed lines represent the confinement loss in the y polarization and x polarization directions, respectively. Due to the addition of the limitation of bandwidth, there is a shift in the resonance wavelength of the 5th and 15th generations and accompanied by irregular changes in the confinement loss peak across all generations. But finally, in the 15th generation, the maximum value of the confinement loss is obtained. At this time, it corresponds to the intersection of the effective refractive indices in Fig. 9(b). The point is exactly at 1.55 μm.

For the fiber length of 1000 nm, the trend of the CT value is almost the same as the value of confinement loss, and there is only a difference in the peak, as shown in Fig. 10. In the 15th generation, the value of CT is higher than 20 dB for the wavelength from around 1.20 μm to 2.0 μm meaning that the resulting bandwidth of CT is about more than 800 nm. The CT peak value at this time is 1845.3113 dB. Additionally, the wider bandwidth and higher peak value of CT can be achieved with the increase of the fiber length at 1.55 μm. Although the proposed filter can maintain more than 800 nm bandwidth for larger fiber lengths, we have considered fiber length of 1000 nm to make the device more compact, capable of sustaining broad bandwidth of around 800 nm with CT higher than 20 dB.

Table IV lists the data for the original reference structure, univariate and bivariate analysis. It is clear that the diameter of gold-coated holes (d_1), the diameter of the air holes on the left and right sides of the fiber core (d_2) and the thickness of gold

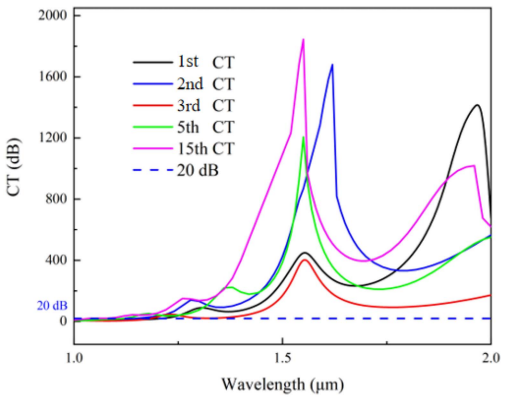

Fig. 10. The CT and bandwidth for 1000 nm fiber length of the 1st, 2nd, 3rd, 5th and 15th generations.

TABLE IV
STATISTICS OF THE STRUCTURE PARAMETERS

parameter	Reference structure	Univariate Analysis	Bivariate Analysis
s (μm)	3.1	3.1	3.1
t (nm)	23	21	21
p (μm)	1.95	1.87	1.94
d_1 (μm)	1.6	1.7	1.8
d_2 (μm)	1.7	1.5	1.7
d_3 (μm)	1.4	1.4	1.5
d_4 (μm)	1.0	1.0	1.0
CT (dB)	1375.94	1775.4735	1845.3113
Bandwidth(nm)	900	850	800

film (t) are particularly critical and the rate of change is 12.5%, 11.8% and 8.7%, respectively. The influence of other parameters is clearly less. These results illustrate that, in fabrication, more attention needs to be paid to the central structure and metal layer thickness rather than the peripheral parts.

The fabrication tolerances analysis is of great significance. Generally, the variation of $\pm 1\%$ in the value of the structural parameters is considered acceptable during the fabrication process. Table V analyzes the characteristics of the filter by changing the values of the optimized structural parameters by 2%. It can be seen that the change of air hole parameters d_1, d_2, d_3 and d_4 and the thickness of gold film t can barely impact filtering performance. However, exceeding the upper limit may result in overlap between adjacent pores, while reduction beyond the lower limit is difficult to achieve. When s increases by 2%, the resonance wavelength shifts from 1550 nm to 1545 nm, and the CT value reaches 1069.2482 dB/cm. Valid data cannot be extracted when s is reduced by 2% because of the size constraints of the PCF geometry structure. In summary, the filter can achieve great separation in the x and y directions with excellent fabrication tolerance. Thus, it is concluded that GA algorithm is applied well enough to determine the geometric parameter values of the PCF polarization filter from the optical properties, and its performance can match the traditional numerical simulation method.

Eventually, in order to demonstrate the scientific validity of this work, the optimized polarization filter is compared with

TABLE V
FABRICATION TOLERANCE OF PROPOSED PCF FILTER

parameter	The fabrication tolerance analysis	Resonance wavelength of y-pol(μm)	CL of y-pol/(dB/cm)
s (μm)	+2%	1.545	1069.2482
	-2%	-	-
t (nm)	+2%	1.500	1834.9835
	-2%	1.525	1861.7124
d_1 (μm)	+2%	1.515	1909.5289
	-2%	1.535	1778.2319
d_2 (μm)	+2%	1.525	1830.8862
	-2%	1.515	1793.2814
d_3 (μm)	+2%	1.520	1817.5494
	-2%	1.555	1816.1615
d_4 (μm)	+2%	1.540	1864.8992
	-2%	1.560	1820.2335

TABLE VI
COMPARISON WITH THE PCF POLARIZATION FILTERS ALREADY REPORTED

Ref.	Resonance Wavelength (μm)	Length (nm)	CT (dB)	Bandwidth (nm)
[29]	1.55	1000	−290.27	530
[30]	1.55	1000	326.7	480
[31]	1.55	1000	806.52	380
[32]	1.55	1000	843.62	630
This work	1.55	1000	1845.31	800

previously reported ones in terms of resonance wavelength, fiber length, CT value and bandwidth in Table VI. According to the results shown in Table VI, our work has achieved larger CT values and wider bandwidths than the published polarization filters at the 1.55 μm resonance wavelength with the fiber length of 1000 nm. From this comparison, the optimized PCF polarization filter has a high CT superior to others and broader bandwidth than most devices, which provides a reference for the design and fabrication of other devices.

IV. CONCLUSION

In this work, the selection of the geometric parameters of the PCF polarization filter is optimized by using GA. The geometric parameters of the optimized PCF polarization filter are $s = 3.1\,\mu$m, $t = 21$ nm, $p = 1.94\,\mu$m, $d_1 = 1.8\,\mu$m, $d_2 = 1.7\,\mu$m, $d_3 = 1.5\,\mu$m, $d_4 = 1.0\,\mu$m. The CT and bandwidth are greater than 1845.3113 dB and 800 nm, which demonstrates that the optimized method adopted in this paper has excellent optimization ability. The use of GA method has greatly expanded the range of the choice of the initial structures and saved the workforce and time, which cannot be achieved by numerical simulation methods. In addition, the proposed GA has a high potential for optimization, analysis and fabrication of the PCF polarization filter or other optical devices.

REFERENCES

[1] F. Poli, A. Cucinotta, and S. Selleri, *Photonic Crystal Fibers: Properties and Applications*. Berlin, Germany: Springer, vol. 102, 2007.

[2] G.-B. Yin, S.-G. Li, S. Liu, and X.-Y. Wang, "The optimization of dispersion properties of photonic crystal fibers using a real-coded genetic algorithm," *Chin. Phys. Lett.*, vol. 28, no. 6, 2011, Art. no. 064215.

[3] M. A. Mollah, M. A. Mazid, and K. Ahmed, "Hi-Bi photonic crystal fiber for broadband filter realization using copper microwires," *Plasmonics*, vol. 15, no. 6, pp. 1789–1797, 2020.

[4] Z. Qiao, X. Pan, F. Zhang, and J. Xu, "A tunable dual-band metamaterial filter based on the coupling between two crossed SRRs," *IEEE Photon. J.*, vol. 13, no. 3, Jun. 2021, Art. no. 4600207.

[5] Z. Yu, Z. Jin, T. Lv, and L. Liu, "High extinction ratio and large bandwidth PCF polarization filter with gold-wires coated by monocrystalline silicon," *IEEE Photon. J.*, vol. 14, no. 4, Aug. 2022, Art. no. 6843806.

[6] S. Chugh, A. Gulistan, S. Ghosh, and B. M. A. Rahman, "Machine learning approach for computing optical properties of a photonic crystal fiber," *Opt Exp.*, vol. 27, no. 25, pp. 36414–36425, Dec. 2019.

[7] A. Zelaci, A. Yasli, C. Kalyoncu, and H. Ademgil, "Generative adversarial neural networks model of photonic crystal fiber based surface plasmon resonance sensor," *J. Lightw. Technol.*, vol. 39, no. 5, pp. 1515–1522, 2021.

[8] J. Jiang, M. Chen, and J. A. Fan, "Deep neural networks for the evaluation and design of photonic devices," *Nature Rev. Mater.*, vol. 6, no. 8, pp. 679–700, 2020.

[9] L. Gao, Y. Chai, D. Zibar, and Z. Yu, "Deep learning in photonics: Introduction," *Photon. Res.*, vol. 9, no. 8, pp. DLP1–DLP3, 2021.

[10] F. Ye, C. Doerr, H. Wang, and T. Back, "Automated configuration of genetic algorithms by tuning for anytime performance," *IEEE Trans. Evol. Comput.*, early access, Mar. 14, 2022, doi: 10.1109/TEVC.2022.3159087.

[11] C. Tao, X. Wang, F. Gao, and M. Wang, "Fault diagnosis of photovoltaic array based on deep belief network optimized by genetic algorithm," *Chin. J. Elect. Eng.*, vol. 6, no. 3, pp. 106–114, Sep. 2020.

[12] J. H. Lu, D. P. Cai, Y. L. Tsai, C. C. Chen, C. E. Lin, and T. J. Yen, "Genetic algorithms optimization of photonic crystal fibers for half diffraction angle reduction of output beam," *Opt Exp.*, vol. 22, no. 19, pp. 22590–22597, Sep. 2014.

[13] F. R. Arteaga-Sierra, C. Milian, I. Torres-Gomez, M. Torres-Cisneros, G. Molto, and A. Ferrando, "Supercontinuum optimization for dual-soliton based light sources using genetic algorithms in a grid platform," *Opt Exp.*, vol. 22, no. 19, pp. 23686–23693, Sep. 2014.

[14] Y. Huang, Z. Zhen, Y. Shen, C. Min, and G. Veronis, "Optimization of photonic nanojets generated by multilayer microcylinders with a genetic algorithm," *Opt Exp.*, vol. 27, no. 2, pp. 1310–1325, Jan. 2019.

[15] B. Dahanayake, "Maxwell's equations and propagation of light: Not relative," *Int. J. Astrophys. Space Sci.*, vol. 3, no. 6, 2015, Art. no. 78.

[16] N. Chen, X. Zhang, M. Chang, X. Lu, and J. Zhou, "Broadband plasmonic polarization filter based on photonic crystal fiber with dual-ring gold layer," *Micromachines (Basel)*, vol. 11, no. 5, Apr. 2020, Art. no. 470.

[17] Q. Liu, S. Li, and H. Chen, "Two kinds of polarization filter based on photonic crystal fiber with nanoscale gold film," *IEEE Photon. J.*, vol. 7, no. 1, Feb. 2015, Art. no. 2700210.

[18] C. Liu et al., "The single-polarization filter composed of gold-coated photonic crystal fiber," *Phys. Lett. A*, vol. 383, no. 25, pp. 3200–3206, 2019.

[19] C. Peng, X. Wu, W. Yuan, X. Zhang, Y. Zhang, and Y. Li, "MGRFE: Multilayer recursive feature elimination based on an embedded genetic algorithm for cancer classification," *IEEE/ACM Trans. Comput. Biol. Bioinf.*, vol. 18, no. 2, pp. 621–632, Mar./Apr. 2021.

[20] A. Krohn, S. Pachnicke, and P. A. Hoeher, "Genetic optimization of liquid crystal matrix based interference suppression for VLC MIMO transmissions," *IEEE Photon. J.*, vol. 14, no. 1, Feb. 2022, Art. no. 7300705.

[21] H. Chen, H. Yong, and Y. Zhou, "Crack detection in bulk superconductor using Genetic Algorithm," *Eng. Fracture Mech.*, vol. 265, 2022, Art. no. 108372.

[22] H. Li et al., "Generation of focal patterns with uniform intensity distribution from speckle by Hadamard-genetic algorithm," *IEEE Photon. J.*, vol. 13, no. 3, Jun. 2021, Art. no. 5000108.

[23] Y. Wang, J. Wu, Z. Wang, C. Huang, H. Y. Fu, and Q. Li, "Optimization of epsilon-near-zero multilayers for near-perfect light absorption using an enhanced genetic algorithm," *IEEE Photon. J.*, vol. 13, no. 5, Oct. 2021, Art. no. 5700110.

[24] D. Yang, Z. Wei, B. Xu, and T. Cheng, "Design of an asymmetric gold-coated photonic crystal fiber (PCF) polarization filter based on surface plasmon resonance (SPR)," *Instrum. Sci. Technol.*, vol. 50, pp. 306–320, 2021.

[25] Y.-L. Yu, H. Kishikawa, S.-K. Liaw, M. Adiya, and N. Goto, "Broadband silicon core photonics crystal fiber polarization filter based on surface plasmon resonance effect," *Opt. Commun.*, vol. 482, 2021, Art. no. 126587.

[26] N. Isik and M. Ince, "Determination of electron trajectories within an energy analyzer using by a genetic algorithm method," *Optik*, vol. 260, 2022, Art. no. 169076.

[27] E. Kerrinckx et al., "Photonic crystal fiber design by means of a genetic algorithm," *Opt. Exp.*, vol. 12, no. 9, pp. 1990–1995, 2004.

[28] W. Q. Zhang, S. Afshar, and T. M. Monro, "A genetic algorithm based approach to fiber design for high coherence and large bandwidth supercontinuum generation," *Opt. Exp.*, vol. 17, no. 21, pp. 19311–19327, 2009.

[29] Y. Wang, S. Li, M. Wang, and P. Yu, "Refractive index sensing and filtering characteristics of side-polished and gold-coated photonic crystal fiber with a offset core," *Opt. Laser Technol.*, vol. 136, 2021, Art. no. 106759.

[30] Y. Guo, J. Li, S. Li, S. Zhang, and Y. Liu, "Broadband single-polarization filter of D-shaped photonic crystal fiber with a micro-opening based on surface plasmon resonance," *Appl. Opt.*, vol. 57, pp. 8016–8022, 2018.

[31] R. A. Shima, M. A. Mollah, and M. Y. Ali, "Au-ITO deposited D-shaped photonic crystal fiber polarizer with a micro-opening based on surface plasmon resonance," *Optik*, vol. 224, 2020, Art. no. 165489.

[32] Y. Liu et al., "Design of a single-polarization filter based on photonic crystal fiber with gold film on the inner wall of two ultra-large holes," *Opt. Laser Technol.*, vol. 114, pp. 114–121, 2019.